

Global *ab initio* potential energy surface for the $O_2(^3\Sigma_g^-) + N_2(^1\Sigma_g^+)$ interaction. Applications to the collisional, spectroscopic, and thermodynamic properties of the complex

Massimiliano Bartolomei, Estela Carmona-Novillo, Marta I. Hernández, José Campos-Martínez
*Instituto de Física Fundamental, (IFF-CSIC) Consejo Superior
de Investigaciones Científicas, Serrano 123, 28006 Madrid, Spain*

Robert Moszyński
*Quantum Chemistry Laboratory, Faculty of Chemistry,
University of Warsaw, L. Pasteura 1 02-093 Warszawa, Poland*

A detailed characterization of the interaction between the most abundant molecules in air is important for the understanding of a variety of phenomena in atmospheric science. A completely *ab initio* global potential energy surface (PES) for the $O_2(^3\Sigma_g^-) + N_2(^1\Sigma_g^+)$ interaction is reported for the first time. It has been obtained with the symmetry-adapted perturbation theory utilizing a density functional description of monomers [SAPT(DFT)] extended to treat the interaction involving high-spin open-shell complexes. The computed interaction energies of the complex are in a good agreement with those obtained by using the spin-restricted coupled cluster methodology with singles, doubles and noniterative triple excitations [RCCSD(T)]. A spherical harmonics expansion containing a large number of terms due to the anisotropy of the interaction has been built from the *ab initio* data. The radial coefficients of the expansion are matched in the long range with the analytical functions based on the recent *ab initio* calculations of the electric properties of the monomers [M. Bartolomei et al., J. Comp. Chem., **32**, 279 (2011)]. The PES is tested against the second virial coefficient $B(T)$ data and the integral cross sections measured with rotationally hot effusive beams, leading in both cases to a very good agreement. The first bound states of the complex have been computed and relevant spectroscopic features of the interacting complex are reported. A comparison with a previous experimentally derived PES is also provided.

I. INTRODUCTION

Simple molecular gases interact in our atmosphere and the outer space through weak intermolecular forces giving rise to many different processes that roughly speaking are characterized by the energy transfer and momentaneous rearrangements of their isolated charge distributions. It is, therefore, of a paramount interest an accurate description of these weak interactions and properties that appear as a consequence. Among these simple molecular species, O_2 and N_2 are central because of their abundance in our atmosphere, and their importance for life.

Another important consequence of the weak intermolecular forces is the existence of weakly bound complexes, mainly dimers. In some cases as, in the O_2 dimer, its existence was already suggested as early as 1924 when Lewis[1] proposed the existence of a strong bond between two oxygen molecules. In search of such a dimer Welsh et. al[2] found much stronger and universal bands, which are known as Collision-Induced Absorption[3] (CIA). Both the dimeric complex and CIA are close and related phenomena that are important not only for spectroscopic purposes[4], but for the energy transfer rates and other observables that are key ingredients in the atmospheric modeling[5] and many other areas in which the delicate balance between radiative and non-radiative processes is necessary to reach an acceptable agreement with observation.

Since the importance of the previously mentioned effects are intimately related to the gas density, the knowl-

edge of an accurate potential energy surface (PES) that could describe short and long-range behavior at once becomes evident.

For the oxygen dimer, we have recently succeeded in producing a global potential energy surface with *ab initio* calculations at a high level of theory. In particular, for the quintet state multiplicity a restricted coupled-cluster theory with singlet, doubles, and perturbative triple excitations [RCCSD(T)] was successfully used[6] to compute this PES. This state is well represented by a single configuration while the singlet and triplet states are inherently multiconfigurational and therefore the CCSD(T) cannot be applied. A scheme was proposed[7] to sort out this problem that was based on a difference procedure involving multireference electronic structure methods. The result is a global potential energy surface[8] that yields excellent results as compared with all experimental data available and both for the short and long range[9]. In the case of the nitrogen dimer, although it is not an open-shell system it was not easy to accomplish an accurate description until recently. Currently, there are several *ab initio* PES[10] that have been computed using Symmetry Adapted Perturbation Theory (SAPT)[11], and that have been very recently used[12] to study CIA for nitrogen.

The data for the heterodimer $N_2 - O_2$ are scarcer, even though an accurate description of the interactions is of primordial relevance to interpret data from observation and remote sensing and atmospheric modeling. One of the few available PES is an experimentally derived po-

tential energy surface[13] (Perugia-PES, from now on), which was obtained from molecular beam experiments and gives an excellent answer when compared with available experimental data.

Here, we employ SAPT(DFT) to calculate for the first time an accurate *ab initio* PES that is further expanded in order to have a functional form ready to use in dynamical calculations. The performance of the newly computed PES is compared with previous ones as well as tested against experimental data. It should be stressed that the SAPT(DFT) approach is particularly well suited for the calculations of global potential energy surfaces for weakly bound complexes. As shown in Ref. [14] the accuracy of the SAPT(DFT) results is often comparable to RCCSD(T), while the computational cost is much lower.

The paper is organized as follows. Section II gives the details of the PES calculations, including the angular expansion and the long-range behavior. In Section III we discuss the topography of the potential energy surface and compare the computed second virial coefficients and integral cross sections with the available experimental data. In Section IV we report calculations of the bound rovibrational levels. Finally, in Section V we conclude our paper.

II. THE O₂-N₂ PES: CALCULATIONS

Diatom-diatom Jacobi vectors, \mathbf{r}_a , \mathbf{r}_b and \mathbf{R} , are used, where \mathbf{r}_a and \mathbf{r}_b are the interatomic vectors of O₂ and N₂, respectively, and \mathbf{R} is the vector joining the centers of mass of the diatoms. Thus, the six internal coordinates determining the O₂-N₂ PES are the distances R , r_a , and r_b , and θ_a , θ_b , and ϕ , the angles formed by \mathbf{R} and \mathbf{r}_a , \mathbf{R} and \mathbf{r}_b , and the torsional angle, respectively. In the PES reported here, the intramolecular distances have been fixed at the O₂ and N₂ equilibrium distances, $r_a = 2.28$ and $r_b = 2.08$ bohr, respectively, so that we describe the interaction between the diatoms in their ground vibrational states.

As done previously[6, 8] we have considered the geometries generated from 9 Gauss-Legendre quadrature points in the $-1 \leq \cos\theta_a, \cos\theta_b \leq 1$ range and from 5 Gauss-Chebyshev points for $0 \leq \phi \leq \pi$. An initial range in the torsional angle from $[0; 2\pi]$ has been reduced to $[0; \pi]$ by use of the permutation-inversion symmetry of this system[15], which also allows us to reduce the initial $9 \times 9 \times 5$ grid to a $5 \times 5 \times 5$ grid ($-1 \leq \cos\theta_a, \cos\theta_b \leq 0$). If we further consider the following equivalences due to symmetry $(\theta_a, \pi/2, \phi) \equiv (\theta_a, \pi/2, \pi - \phi)$ and $(\pi/2, \theta_b, \phi) \equiv (\pi/2, \theta_b, \pi - \phi)$, we are finally left with 107 “irreducible” geometries. For each angular arrangement, 18 points in the intermolecular coordinate R , ranging from 16.0 to 5.0 bohr, were considered.

TABLE I. Energies (in meV) for five limiting configurations at intermolecular distances close to the minima (in parenthesis, in bohr), as obtained from SAPT(DFT) with aug-cc-pVTZ and aug-cc-pVQZ basis sets plus bond functions (the same in both cases, see text).

	H (6.5)	X (6.5)	T _a (7.5)	T _b (7.5)	L (8.5)
VTZ	14.344	14.685	14.004	12.580	9.324
VQZ	14.549	14.909	14.104	12.723	9.322

A. SAPT(DFT) *ab initio* calculations

Since the O₂ and N₂ monomers have electronic spins $S_a = 1$ and $S_b = 0$, respectively, the intermolecular potential does not depend on the spin couplings between the monomers and therefore accurate single reference approaches, such as SAPT(DFT) and spin-restricted RCCSD(T), can be applied. The SAPT(DFT) calculations were performed using the methodology of Ref. [14] which is suitable to obtain the interactions in high-spin dimers formed by open-shell monomers. The aug-cc-pVTZ and aug-cc-pVQZ basis sets[16], both supplemented by the bond function set [3s3p2d1f] developed by Tao[17] and placed in the middle of the intermolecular distance, have been used in the calculations. The monomer DFT calculations employed the PBE0 hybrid functional[18] and were done using the DALTON[19] program. We applied the Fermi-Amaldi-Tozer-Handy asymptotic correction[20, 21] with the ionization potentials of 0.479 and 0.613 a.u.[22] (for α and β electrons, respectively) for O₂ and 0.5726 a.u.[23] for N₂. The SAPT(DFT) calculations used the open-shell SAPT(DFT) program of the SAPT2008 code [24].

First, we have tested the basis set saturation and performances for some limiting configurations of the interacting complex: linear ($D_{\infty h}$), T-shaped (C_{2v}), rectangular (D_{2h}) and crossed (D_{2d}) arrangement, in the following, referred to as L, T, H and X, respectively. We distinguish two T-shaped orientations: T_a, where the O₂ intramolecular vector \mathbf{r}_a is perpendicular to \mathbf{R} , and T_b, where N₂ is the diatom oriented perpendicularly to the intermolecular vector. Results are reported in Table I. As can be noticed both sets provide almost identical results: the largest differences, corresponding to H and X configurations, are within 1 %. The analysis was extended to other intermolecular distances and it was found that the discrepancies between both basis sets remain of the same order of magnitude. We regard these deviations as acceptable, bearing in mind that for a single geometry on a single processor the aug-cc-pVTZ calculations are three times faster than those employing the larger basis set.

In order to further check the performance of the SAPT(DFT) results, supermolecular spin-restricted RCCSD(T)/aug-cc-pVTZ (plus bond functions) calculations have been performed for the same limiting configurations. The counterpoise method[25, 26] was applied to correct for the basis set superposition error and the

calculations were carried out with the MOLPRO2006.1 package[27]. The comparison between the interaction energies obtained from the two different levels of theory are shown in Fig. 1. It can be noticed that SAPT(DFT) curves are somewhat more attractive in the well region for the most attractive configurations (H, X and T_a), while they are slightly more repulsive for the remaining arrangements (T_b and L). Overall the agreement can be termed as good since discrepancies are in general within 5 %. It is noteworthy to stress the saving in computing time provided by the SAPT(DFT) methodology. In fact we have estimated that for a single point/single CPU, RCCSD(T) calculations would be about six times slower than equivalent SAPT(DFT) ones if no symmetry is used (as it is for most of the geometrical arrangements).

Supported by the above mentioned tests we decided to choose the SAPT(DFT) methodology with the aug-cc-pVTZ basis supplemented with the [3s3p2d1f] set of bond functions for all the geometries needed to obtain a complete and reliable representation of the O₂-N₂ PES.

B. Spherical harmonics expansion

The interaction potential V is written using a spherical harmonics expansion as[28]:

$$V(R, \theta_a, \theta_b, \phi) = (4\pi)^{3/2} \sum_{l_a, l_b, l} f^{l_a l_b l}(R) A_{l_a l_b l}(\theta_a, \theta_b, \phi), \quad (1)$$

with

$$A_{l_a l_b l}(\theta_a, \theta_b, \phi) = \left(\frac{2l+1}{4\pi}\right)^{1/2} \sum_m \begin{pmatrix} l_a & l_b & l \\ m & -m & 0 \end{pmatrix} Y_{l_a, m}(\theta_a, 0) Y_{l_b, -m}(\theta_b, \phi), \quad (2)$$

where $Y_{l_a, m}$ and $Y_{l_b, -m}$ are the normalized spherical harmonics that are coupled with a $3j$ symbol, and m runs from $-\min(l_a, l_b)$ to $\min(l_a, l_b)$. The radial coefficients $f^{l_a l_b l}(R)$ are computed by integrating V over the angular variables:

$$f^{l_a l_b l}(R) = \pi^{1/2} \int_{-1}^1 d(\cos \theta_a) \int_{-1}^1 d(\cos \theta_b) \int_0^{2\pi} d\phi V(R, \theta_a, \theta_b, \phi) A_{l_a, l_b, l}^*(\theta_a, \theta_b, \phi). \quad (3)$$

Integrals were carried out for each intermolecular distance R by means of Gauss-Legendre (for $\cos\theta_{a,b}$) and Gauss-Chebyshev (for ϕ) quadratures[29].

Due to the permutation-inversion symmetries of the complex, l_a , l_b , and l integers must be even. In contrast with dimers of identical diatoms, however, $f^{l_a l_b l}$ and $f^{l_b l_a l}$ coefficients differ. From the set of quadrature points used in the present work, a series of 85 different radial coefficients arise, consisting in all the combinations

TABLE II. Comparison of *ab initio* energies with those resulting from the spherical harmonic expansion of Eq. 1 using the set of 39 radial coefficients detailed in the text, for several orientations and intermolecular distances.

Geometry			R	$V_{abinitio}$	$V_{expanded}$	%
θ_a	θ_b	ϕ	(bohr)	(meV)	(meV)	
(degrees)						
			5.25	71.30	71.63	0.46
	H		5.50	28.10	28.08	0.07
90	90	0	6.25	-12.77	-12.84	0.55
			6.50	-14.34	-14.37	0.66
			7.00	-12.75	-12.75	0.21
			12.00	-0.513	-0.513	0.00
			14.00	-0.192	-0.192	0.00
			5.25	57.20	55.25	3.41
	X		5.50	20.64	20.02	3.00
90	90	90	6.25	-13.59	-13.50	0.66
			6.50	-14.69	-14.63	0.41
			7.00	-12.80	-12.78	0.16
			12.00	-0.546	-0.546	0.00
			14.00	-0.209	-0.209	0.00
			5.25	577.57	577.84	0.05
	T _a		5.50	341.08	340.70	0.11
90	0	0	7.25	-13.52	-13.52	0.00
			7.50	-14.00	-14.01	0.07
			8.00	-11.85	-11.85	0.00
			12.00	-0.954	-0.954	0.00
			14.00	-0.351	-0.351	0.00
			5.25	661.64	660.63	0.15
	T _b		5.50	389.72	388.71	0.26
0	90	0	7.25	-11.57	-11.56	0.09
			7.50	-12.58	-12.57	0.08
			8.00	-11.01	-11.00	0.09
			12.00	-0.928	-0.928	0.00
			14.00	-0.350	-0.350	0.00
			5.25	3332.44	3344.74	0.37
	L		5.50	2381.61	2384.07	0.10
0	0	0	8.25	-8.35	-8.33	0.24
			8.50	-9.32	-9.31	0.11
			9.00	-8.20	-8.21	0.12
			12.00	-1.129	-1.128	0.09
			14.00	-0.361	-0.361	0.00
			5.25	626.06	626.54	0.08
	S ₄₅		5.50	386.29	386.37	0.02
45	45	0	7.25	-9.40	-9.38	0.21
			7.50	-11.40	-11.40	0.00
			8.00	-10.84	-10.84	0.00
			12.00	-0.945	-0.946	0.11
			14.00	-0.349	-0.349	0.00

($l_a l_b l$) where $l_a, l_b = 0, \dots, 8$ and $|l_a - l_b| \leq l \leq l_a + l_b$. We have selected a subset of 39 radial coefficients for which the interaction potential is sufficiently well represented. It was built by discarding, for $l_a > 4$ or $l_b > 4$, all coefficients with $l \neq l_a + l_b$, except for ($l_a l_b l$) = (2 6 4), (2 6 6), (6 2 4) and (6 2 6). Root mean square (rms) relative and absolute errors of this expansion with respect to the *ab initio* energies (for all distances and quadrature points) are about 2 % and 0.55 meV, respectively.

A further indication of the quality of the spherical harmonics expansion is given in Table II, where a comparison between *ab initio* interaction energies and those corre-

sponding to the expansion is given for some selected geometries. This is an independent check of the accuracy of the expansion, since, except for the X geometry, none of these geometries correspond to the Gaussian quadrature points used to build the PES and then, they were computed independently. It can be seen that the comparison is satisfactory. The largest discrepancies are found at short intermolecular distances ($R \leq 5.5$ bohr) where the interaction becomes more anisotropic.

C. Long range behavior and matching procedure

In this paragraph we present the asymptotic extension of the PES by using analytical expressions for the long range behavior. Following the Rayleigh-Schrödinger perturbation theory of intermolecular forces [30] in the multipole approximation [31, 32], the radial coefficients $f^{l_a l_b l}(R)$ of Eq. 1 can be written by a sum of electrostatic (e l), dispersion (d) and induction (i) contributions:

$$f^{l_a l_b l}(R) = f_{el}^{l_a l_b l}(R) + f_d^{l_a l_b l}(R) + f_i^{l_a l_b l}(R), \quad (4)$$

where

$$f_{el}^{l_a l_b l}(R) = \delta_{l_a+l_b, l} \left[\frac{(2l_a + 2l_b)!}{(2l_a + 1)!(2l_b + 1)!} \right]^{1/2} \frac{Q_0^{l_a} Q_0^{l_b}}{R^{l_a+l_b+1}}, \quad (5)$$

and

$$f_{(d,i)}^{l_a l_b l}(R) = - \frac{1}{[(2l_a + 1)(2l_b + 1)(2l + 1)]^{1/2}} \sum_n \frac{C_{n,(d,i)}^{l_a l_b l}}{R^n}. \quad (6)$$

Coefficients involved in Eqs. 5 and 6 have recently been obtained from high level *ab initio* calculations[9]. Permanent electric multipole moments Q_0^l ($l=2,4,6,8$) were taken from Tables III and IV of Ref.[9], and dispersion and induction coefficients $C_{n,(d,i)}^{l_a l_b l}$, (with $n=6,8$ and $n=8$, respectively, and $(l_a l_b l)$ up to $(2\ 4\ 6)$), from Table VII of the same work.

The expression of Eq. 4 was used for distances $R \geq 19$ bohr. For shorter distances, $f^{(l_a l_b l)}(R)$ were calculated from cubic spline interpolation of the values $f_i^{(l_a l_b l)}$ obtained from the SAPT(DFT) calculations at the set of distances $R_i, i = 1, \dots, N$. An additional point $R_{N+1}=19$ bohr was included in that grid with a value given by Eq. 4. The analytical derivative of $f^{l_a l_b l}(R)$ at R_{N+1} was used as a boundary condition for solving the interpolation equations, so that a smooth behavior of the radial term around R_{N+1} is achieved. The procedure worked well, providing a good indication of the consistency between the SAPT(DFT) calculations and the computed electric properties of the molecular fragments. As an example, we show in Fig.2 the behavior of the first four coefficients around the matching region. In there the long

TABLE III. Equilibrium distances R_m (in bohr) and well depths D_m (in meV) of the O₂-N₂ PES at some selected orientations as well as the spherical average. Present results are compared with those of Perugia-PES[13].

	Ref.[13]		This work	
	D_m	R_m	D_m	R_m
H	14.89	6.99	14.41	6.56
X	16.08	6.92	14.63	6.52
T _a	12.17	7.54	14.05	7.44
T _b	12.45	7.58	12.58	7.52
L	6.52	8.47	9.33	8.54
S ₄₅	8.76	8.01	11.68	7.66
f^{000}	10.90	7.60	10.04	7.62

range behavior of f^{000} from the Perugia-PES[13] is also reported.

III. RESULTS AND DISCUSSION

A. The potential energy surface

In Fig. 3 and Table III, we report the most prominent features of the present PES in comparison with those of the Perugia-PES[13]. Both intermolecular potentials are in a good qualitative agreement. For example, the crossed configuration (X) is the most stable geometry for both PESs, while a good match in the equilibrium distance and well depth of the spherically averaged interaction is observed. Nevertheless, some important differences can be found when going into details. In fact, present calculations give shorter equilibrium distances for the parallel (H) and the crossed (X) configurations, the curves being almost identical for these two orientations. Moreover, the *ab initio* well depth of the T_a geometry is larger than the T_b one, and it is very close to those of the most stable X and H arrangements. This is in contrast with the features of the T-shaped geometries of the Perugia-PES[13] (see the intermediate panel of Fig. 3). In general, the present PES provides deeper potentials for the more repulsive geometries (T-shaped and collinear L), while for the most attractive ones (X and H), slightly shallower wells. In spite of this, we believe that the *ab initio* PES is more anisotropic since, at a given R , the interaction energy exhibits a stronger dependence with the angles than in the Perugia-PES case.

The *ab initio* spherically averaged radial term (f^{000}) is compared with that of Ref.[13] in the lower panel of Fig. 3. This test is meaningful because the latter was obtained from analyses of accurate integral cross section data[33]. As can be seen, although present calculations slightly underestimate the experimentally derived interaction energy in the well and repulsive regions, the matching for

the equilibrium distance, R_m , is very good (see Table III). Differences in the interaction energy are less than 1 meV near the equilibrium distance and become almost negligible in the long range tail (see also Fig. 2).

More insight into the features of the O_2-N_2 interaction is gained from Fig. 4, where we show a few representative pathways joining the most stable configurations X, T_a , T_b , and H. First, it is worthwhile noticing the almost flat path between the H and X geometries, suggesting a free internal (torsional) rotation in the dimer. In addition, it can be seen that the paths connecting the T-shaped structures with the most stable H or X geometries involve very small barriers (except for the T_a -H path). This finding brings a picture of the O_2-N_2 dimer as a rather floppy cluster.

B. Integral cross sections

In order to assess the reliability of the present PES, we have tested it against available experimental data such as the total integral cross sections reported in Refs. [13, 33] for the scattering of rotationally hot and near effusive O_2 beams. In these experiments, oxygen projectiles are at a high rotational temperature (about 10^3 K) and collide with target N_2 molecules which are in the scattering chamber at low translational temperature. Under these conditions Brunetti et al. [33] were able to resolve the glory structure which in turn can give valuable information[34–36] on the intermolecular interaction involved. As explained before (see Ref. [13] and references therein), at low collision velocities, the colliders mainly probe the isotropic component of the interaction, while the anisotropy plays an increasing role at intermediate and high velocities.

Accordingly, we have computed total cross sections $Q(v)$ using two different schemes. In one case, we have used just the first term of the expansion of Eq. 1, f^{000} , which represents the spherical average of the PES. In a second approach, we have used the potential energy surface in an atom-diatom limit, corresponding to the interaction averaged over the orientation of the O_2 projectile[13]. In the latter case, the surface reduces to the sum of just five terms arising in Eq. 1 when the $(l_a, l_b, l) = (0, l_b, l_b)$ constraint is imposed ($l_b=0,2,4,6,8$) and the calculations were performed using the infinite-order-sudden (IOS) approximation. In both approaches the phase shifts have been evaluated within the JWKB approximation. The center-of-mass cross sections are then convoluted over the relative velocity distribution and transformed to the laboratory reference frame. More technical details can be found in Ref. [37] and references therein.

In Fig. 5 we report the cross sections obtained within the two proposed schemes and using the *ab initio* PESs, in comparison with those obtained using the experimentally derived PES as well as the experimental results[13]. An overall good agreement is noticed. The average value

of the *ab initio* cross sections is just a few percents lower ($< 2\%$) than the best experimental fit, with the glory pattern slightly shifted towards lower velocities. The IOS results with the effective atom-diatom potential better describe the observed glory oscillations than the isotropic potential. It is generally admitted that the average values of the cross sections contain information about the long-range attraction[38, 39]. In this context and for the velocities probed experimentally, the “long range region” corresponds to intermolecular distances of about 11-14 bohr[40, 41] where a good matching between the present and the experimentally derived PESs was already noted (see Figs. 2 and 3). On the other hand, it is also well known that the glory structures of the cross sections provide information on the potential well area[42, 43]. In addition to this, it has been pointed out recently[44] that anisotropy can also influence the velocity positions of the glory extrema in molecule-molecule scattering. In fact, it can be seen in Fig.5 that the glory extrema shift to higher velocities when one moves from the atom-atom to the atom-diatom approximation. Thus, we expect that the full molecule-molecule scattering calculation would shift the glory pattern towards even higher velocities (as found for O_2-O_2 [44]), eventually bringing theoretical results to a closer agreement with the measurements.

C. Second virial coefficients

A further check of the quality of the present PES is carried out through the computation of the second virial coefficient $B(T)$ as a function of the temperature T . To this end we apply the semiclassical theory based on the expressions for two linear molecules presented by Pack[47] which include the first quantum correction due to the relative translational and rotational motions, including Coriolis coupling.

In Table IV and in Fig. 6 (upper panel), the calculated values of $B(T)$ are compared with the experimental data of Refs.[45, 46], together with those corresponding to the Perugia-PES[13]. A more detailed analysis of the deviations of the calculations with respect to the measurements is given in the lower panel of Fig. 6. It can be seen that, except for the results at $T=87.2$ K, the comparison with the experimental data of Ref.[46] is very good and almost perfect around and above the Boyle temperature ($T \sim 353$ K). In fact, the *ab initio* PES works better in the high temperature region than the experimentally derived PES. These results indicate that the present PES is well characterized, especially in the repulsive region.

The role of the anisotropy can be inferred from the comparison of $B(T)$ obtained using the full PES with a calculation where the anisotropy is neglected just by retaining the isotropic component of the interaction. The results of the latter calculations are shown in parentheses in Table IV. It can be noticed that there are significant differences between the two approaches and that this discrepancy increases as temperature decreases. Interest-

TABLE IV. Calculated and measured values of the second virial coefficient $B(T)$ ($\text{cm}^3 \text{mol}^{-1}$) as a function of temperature (in K). Values corresponding to the contribution given by the spherical component of the interaction are shown in parentheses.

T (K)	PES	Ref.[13]	This work	Experimental
87.2	-241.4	(-206.1)	-225.2 (-172.1)	-247.0 \pm 7 ^a
90.0	-227.1	(-194.2)	-212.0 (-162.1)	
100.0	-185.7	(-159.3)	-173.5 (-132.5)	
110.0	-155.0	(-133.0)	-144.9 (-110.0)	
125.0	-121.4	(-103.8)	-113.5 (-84.9)	
140.0	-97.3	(-82.7)	-90.8 (-66.6)	-96.3 \pm 5 ^a
190.0	-50.7	(-41.2)	-46.8 (-30.2)	-49.6 \pm 4 ^a
220.0	-34.9	(-27.0)	-31.9 (-17.6)	-34.8 \pm 3 ^a
240.0	-27.1	(-19.8)	-24.4 (-11.3)	-25.1 \pm 2 ^a
290.0	-12.9	(-6.9)	-10.9 (0.1)	-13.3 ^b
300.0	-10.9	(-5.0)	-8.9 (1.9)	-11.2 ^b
320.0	-6.9	(-1.5)	-5.2 (5.0)	-7.6 ^b
353.0	-1.7	(3.3)	-0.2 (9.3)	-0.1 \pm 2 ^a
403.0	4.3	(8.9)	5.6 (14.2)	6.1 \pm 3 ^a
455.0	8.9	(13.1)	10.0 (18.0)	10.5 \pm 3 ^a
476.0	10.5	(14.5)	11.5 (19.2)	12.2 \pm 3 ^a
500.0	12.1	(16.0)	13.0 (20.5)	
600.0	17.0	(20.5)	17.8 (24.5)	
700.0	20.3	(23.5)	21.0 (27.2)	
800.0	22.6	(25.6)	23.2 (29.0)	
900.0	24.2	(27.0)	24.8 (30.2)	
1000.0	25.4	(28.1)	26.0 (31.2)	

^a Fostiropoulos *et al*[46]

^b Martin *et al* [45]

ingly, the isotropic approximation as obtained using the *ab initio* PES leads to less negative and more positive $B(T)$ at low and high temperatures, respectively, if compared with the results from the experimentally derived PES. This is due to the less attractive character of the isotropic component for the *ab initio* PES as already discussed above (see also Fig.3). However, the contribution of the anisotropy is more important in the *ab initio* than in the experimentally derived PES, which in turn compensates the isotropic contribution and globally leads to a good agreement with the experimental $B(T)$.

Since second virial coefficient measurements for gas mixtures are in general less accurate than those for pure gases [48] we find useful to provide data for temperatures higher than those considered in the experiments, as shown in Table IV. Based on the previous analysis, we believe that present results for the second virial coefficients $B(T)$ are the best theoretical estimates to date for temperatures higher than 353 K and, for $T > 500$ K, they should be taken as the reference data.

IV. BOUND STATE CALCULATIONS

In this section, we report energies and geometries of the lowest bound states of $\text{O}_2\text{-N}_2$. Since the intramolec-

TABLE V. Energies (in meV and cm^{-1}) of the lowest rotationless ($J=0$) states of $^{16}\text{O}_2\text{-}^{14}\text{N}_2$. The parity of j_a (O_2), j_b (N_2) and l in the wave function expansion is indicated, together with the parity of the total eigenfunctions (including the electronic part) with respect to the operations of the G_8 group, and their symmetry (as in Table A-22, page 393 of Ref.[49]). Allowed states are given in boldface.

Level	$E(\text{meV})$	$E(\text{cm}^{-1})$	$j_a j_b l$	P_{12}	P_{34}	E^*	Sym
0	-10.32	-83.28	<i>e e e</i>	-	+	+	B''_2
1	-9.81	-79.11	<i>o o o</i>	+	-	-	B'_1
2	-9.72	-78.37	<i>o o e</i>	+	-	+	B'_2
3	-9.39	-75.78	<i>e o o</i>	-	-	+	A''_1
4	-9.16	-73.89	<i>o e o</i>	+	+	+	A'_1
5	-8.75	-70.59	<i>e e e</i>	-	+	+	B''_2
6	-8.65	-69.79	<i>e e e</i>	-	+	+	B''_2
7	-8.33	-67.23	<i>o e e</i>	+	+	-	A'_2
8	-8.32	-67.09	<i>o e o</i>	+	+	+	A'_1
9	-8.25	-66.53	<i>e e o</i>	-	+	-	B''_1
10	-8.24	-66.46	<i>e e e</i>	-	+	+	B''_2
11	-8.19	-66.08	<i>e o o</i>	-	-	+	A''_1
12	-8.14	-65.68	<i>e o e</i>	-	-	-	A''_2

ular distances have been fixed in the *ab initio* PES, the diatoms O_2 and N_2 are treated as rigid rotors within the present approach. The Hamiltonian describing the nuclear motion writes -using the previously defined diatom-diatom Jacobi coordinates in a space-fixed (SF) frame as [50, 51]

$$H = -\frac{1}{2\mu R} \frac{\partial^2}{\partial R^2} R + \frac{\hat{\ell}^2}{2\mu R^2} + B_a \hat{\mathbf{J}}_a^2 + B_b \hat{\mathbf{J}}_b^2 + V, \quad (7)$$

where atomic units are used ($\hbar = 1$), μ is the reduced mass of the complex, V is the PES, $B_{a,b}$ are the rotational constants of O_2 and N_2 , respectively, and $\hat{\ell}$, $\hat{\mathbf{J}}_a$ and $\hat{\mathbf{J}}_b$ are the angular momentum operators associated with the rotations of the \mathbf{R} , \mathbf{r}_a , and \mathbf{r}_b vectors, respectively. In this way, the total angular momentum is $\mathbf{J} = \hat{\ell} + \hat{\mathbf{J}}_a + \hat{\mathbf{J}}_b$.

Bound states of the complex were obtained by solving the time-independent Schrödinger equation, as described in Ref.[52]. Eigenfunctions with well defined values of J and M (projection onto the SF z axis) are sought by using a convenient basis set expansion

$$\Psi^{JM}(\mathbf{R}, \hat{\mathbf{r}}_a, \hat{\mathbf{r}}_b) = \sum_{j_a j_b j_{ab} \ell} \frac{g_{j_a j_b j_{ab} \ell}^{JM}(R)}{R} I_{j_a j_b j_{ab} \ell}^{JM}(\hat{\mathbf{R}}, \hat{\mathbf{r}}_a, \hat{\mathbf{r}}_b), \quad (8)$$

where $\hat{\mathbf{R}}, \hat{\mathbf{r}}_a, \hat{\mathbf{r}}_b$ are unit vectors (i.e., $\hat{\mathbf{R}} = \mathbf{R}/R$, etc.) and the angular wavefunctions are [50, 51, 53]

$$I_{j_a j_b j_{ab} \ell}^{JM}(\hat{\mathbf{R}}, \hat{\mathbf{r}}_a, \hat{\mathbf{r}}_b) = \left[[Y_{j_a}(\hat{\mathbf{r}}_a) \otimes Y_{j_b}(\hat{\mathbf{r}}_b)]^{j_{ab}} \otimes Y_{\ell}(\hat{\mathbf{R}}) \right]_{M}^J \quad (9)$$

where the irreducible tensor product of two spherical tensors is given by

$$[T_l \otimes T_{l'}]_L^K = \sum_{k=-l}^l \sum_{k'=-l'}^{l'} \langle l, k; l', k' | L, K \rangle T_l^k T_{l'}^{k'}, \quad (10)$$

and $\langle l, k; l', k' | L, K \rangle$ is the Clebsch-Gordan coefficient.

The molecular symmetry group appropriate for describing the O₂-N₂ dimer is G_8 , a permutation-inversion group generated by the spatial inversion of the nuclear coordinates, E^* , and the permutations of identical nuclei within O₂ and N₂, P_{12} and P_{34} , respectively. The basis functions of Eq.9 are well adapted to these operations, with parities given by $(-1)^{j_a+j_b+\ell}$ [53], $(-1)^{j_a}$ and $(-1)^{j_b}$ for E^* , P_{12} and P_{34} , respectively. To complete the analysis, we have to consider the effect of these operations on the electronic wave function since it depends parametrically on the coordinates of the nuclei. This function, correlating with the ${}^3\Sigma_g^- + {}^1\Sigma_g^+$ limit, is symmetric under all the group operations except for the exchange of the oxygen nuclei, P_{12} , for which it is antisymmetric [54]. Thus, the parity of the *total* wavefunction under P_{12} is $(-1)^{j_a+1}$. In addition, calculations have been carried out for the ¹⁶O nuclei, which have zero spin. Therefore, the total wave function must be symmetric under P_{12} and states with even j_a are forbidden.

Calculations were performed with the BOUND package[55]. The coupled differential equations resulting from substitution of Eq. 8 into the Schrödinger equation were propagated from 5.3 to 12.9 bohr, with a step size of 0.015 bohr using the Manolopoulos modified log-derivative algorithm [56], and eigenvalues were located iteratively by using the Johnson's method[57]. The most abundant ¹⁶O and ¹⁴N isotopes are considered, hence the reduced mass is 14.936928 amu. The rotational constants B_a and B_b are 1.438 and 2.013 cm⁻¹, respectively. An angular basis set with $j_a, j_b \leq 14$ was used. Note that we have computed bound states for *all* the symmetries including forbidden states with even j_a , so that a more detailed understanding of the rovibrational structure of the complex can be achieved. The resulting energy levels are converged to within 10⁻⁴ cm⁻¹ at worst.

In Table V we report the energies of the lowest bound states for total angular momentum $J = 0$, together with their behavior under the operations of the symmetry group. Note that only the states shown in boldface are allowed. It can be noticed that there is a rather large density of states or, in other words, the vibrational motions involved have quite low frequencies. Analysis of the corresponding wave functions confirms the characteristic floppiness of this dimer. They have been obtained following the method of Thornley and Hutson [58], and setting the SF polar angles to $\hat{\mathbf{R}}=(\theta_R, \phi_R)=(0,0)$, $\hat{\mathbf{r}}_a=(\theta_a, \phi_a)=(\theta_a, \phi/2)$ and $\hat{\mathbf{r}}_b=(\theta_b, \phi_b)=(\theta_b, -\phi/2)$. For the three lowest states ($n = 0, 1, 2$), wave functions multiplied by $R (R\Psi)$ are shown in Fig. 7. They all have their largest amplitude for $\theta_a=\theta_b=\pi/2$ and, for these reasons, these wavefunctions are depicted as functions of the inter-

TABLE VI. Energies (in cm⁻¹) and symmetries of the lowest rotationally excited states of ¹⁶O₂-¹⁴N₂. Allowed states are given in boldface.

J=1		J=2		J=3	
cm ⁻¹	Sym	cm ⁻¹	Sym	cm ⁻¹	Sym
-83.120	B₁'	-82.804	B₂'	-82.332	B ₁ ''
-81.492	A₂'	-81.185	A₂'	-80.724	A₂'
-81.485	A₁'	-81.165	A₁'	-80.685	A₁'
-80.366	A ₂ ''	-80.063	A ₁ ''	-79.608	A ₂ ''
-80.358	A ₁ ''	-80.038	A ₂ ''	-79.558	A ₁ ''
-78.952	B ₂ ''	-78.638	B ₁ ''	-78.168	B₂'
-78.211	B ₁ ''	-78.516	B ₂ ''	-78.057	B₁'
-75.624	A ₂ ''	-78.515	B ₁ ''	-78.054	B₂'
-74.240	B ₁ ''	-77.900	B ₂ ''	-77.433	B₁'
-74.235	B ₂ ''	-76.560	B₂'	-76.095	B ₁ ''
		-76.560	B₁'	-76.095	B ₂ ''
		-75.321	A ₁ ''	-74.867	A ₂ ''

molecular distance, R , and the torsional angle, ϕ , having fixed θ_a and θ_b at $\pi/2$. The ground state ($n=0$, Fig. 7(a)) is very delocalized with respect to the torsional motion, with a slight propensity for a X configuration. The first excited state ($n=1$, Fig.7(b)) exhibits a node for $\phi=0$ and has its maximum probability density at the X geometry. The second excited state also corresponds to an excitation of the torsional motion, in this case, the node is at $\phi=\pi/2$ and its geometry matches the H orientation.

The relatively large stability of the T-shape orientations in the O₂-N₂ PES (Fig. 3) is revealed in the structure of the higher excited states. Indeed, the third and fourth excited states have T-shape geometries. Wave functions for these states are presented in Fig. 8. The wave function of the $n=3$ state is depicted as a function of R and θ_b , where the θ_a and ϕ angles have been fixed to $\pi/2$ and 0, respectively (Fig. 8(a)). We have chosen to fix θ_a to $\pi/2$ because a maximum of the probability density is found precisely at this orientation. On the other hand, we have found that the amplitude is quite isotropic with respect to the torsional angle and have just chosen a representative planar configuration ($\phi = 0$). It can be seen that this function displays a node at $\theta_b=\pi/2$ and a maximum amplitude for $\theta_b=0$, corresponding to a T_a configuration. Nevertheless, this angular mode displays a wide amplitude motion, since the amplitude is also significant for displacements out of the T_a geometry. The $n=4$ state has, on the other hand, a T_b geometry. The shape of its wave function as a function of R and θ_a is given in Fig. 8(b), having fixed θ_b and ϕ to $\pi/2$ and 0, respectively. As the previous level, the $n=4$ state is also quite floppy with respect to motions of all the intermolecular degrees of freedom.

Finally, a list of some rotationally excited states ($J= 1, 2$, and 3) is reported in Table VI. It is worthwhile noting that the lowest levels of $J= 1$ and 2 are allowed states and their energies are lower than the lowest allowed states

of $J = 0$ (Table V). This feature was already discussed by Aquilanti *et al* in their study of O_2-N_2 based in the Perugia-PES[13].

Unfortunately, we cannot test present results against experiments as we were not able to find any publication on the spectroscopy of O_2-N_2 . Aquilanti *et al.* [13] reported bound states calculated with their experimentally derived O_2-N_2 PES[59]. They reported $J = 0$ states build up using odd and even values of j for O_2 and N_2 , respectively. The lowest energy levels are -98.1, -88.4 and -83.7 cm^{-1} , which should be compared with the corresponding present levels, -73.9, -67.2 and -67.1 cm^{-1} . As can be seen, differences between the *ab initio* PES and the Perugia-PES, discussed previously, become crucial for a quantitative prediction of the bound spectrum of this complex.

Present results can be also compared with the vibrational structure of the related dimers O_2-O_2 and N_2-N_2 . First, O_2-N_2 bound states are quite different to those of O_2-O_2 in the singlet and triplet spin multiplicities, as, due to exchange interactions involving the two open-shell molecules, they exhibit a preference for the H geometry and are much more rigid[60]. However, the lowest vibrational states of O_2-N_2 are impressively similar to accurate calculations of O_2-O_2 in the quintet multiplicity [6]. In addition, the shape of the associated wave functions is very alike. Finally, comparing with calculations based on an experimentally derived PES for N_2-N_2 [61], it is found that energies of the lowest bound states are rather similar: the three lowest energies are -79.9, -77.4 and -71.1. However, it was found that the ground state has a T-shaped geometry (in accordance with the features of the PES), whereas the first state in O_2-N_2 exhibiting such a geometry is the third vibrationally excited state.

V. CONCLUDING REMARKS

In the present paper state-of-the-art *ab initio* techniques have been applied to compute the ground state potential energy surface for the interaction of rigid N_2 and O_2 molecules in their ground electronic and vibrational states. The main results of this paper can be summarized as follows.

1. The potential energy surface for the $O_2(^3\Sigma_g^-) + N_2(^1\Sigma_g^+)$ complex has a global minimum of 14.63 meV at $R = 6.52$ bohr for the X (D_{2d}) geometry, and local minima of 14.05 meV at $R = 7.44$ bohr and 12.58 meV at $R = 7.52$ bohr for the T_a and T_b geometries, respectively.

2. Symmetry-adapted perturbation theory utilizing the DFT description of the isolated monomers was shown to work very well in comparison with the spin-restricted coupled cluster method with single, double, and noniterative triple excitations.
3. The accuracy of the computed potential was checked by comparison with the empirical potential from the Perugia group fitted to the measured integral cross sections. In general, relatively good agreement between the *ab initio* and empirical surfaces is found, the deviations ranging from 3% for the H geometry to 43% for the weakly bound L geometry. The present potential is more anisotropic than the experimentally derived potential.
4. The *ab initio* potential satisfactorily reproduces the measured integral cross sections. Both the glory oscillations as a function of the beam intensity and the absolute cross sections are in a (semi)quantitative agreement with the experimental data.
5. The *ab initio* potential also works well for the second virial coefficient of the O_2-N_2 mixture. Except for the two lowest temperatures, the present results are well within the experimental error bars leading to the best agreement to date for temperatures higher than the Boyle temperature. Second virial coefficients are also computed at temperatures where measured values are unavailable and, considering the accuracy of the present PES, they can be safely used to guide extrapolations at high temperature.
6. The analysis of the bound states of the complex reveals that the complex is floppy, and the nearly free rotors description is adequate. Unfortunately, no experimental data are available for comparison.

The potential energy surface reported in this work can be employed in future investigations such as studies of collision induced absorption or rotationally energy transfer in collisions.

ACKNOWLEDGMENTS

We thank financial support by Spanish grant FIS2010-22064-C02-02. RM thanks the Foundation for Polish Science for support within the MISTRZ programme. Allocation of computing time by CESGA (Spain) and the COST-CMTS Action CM1002 ‘‘Convergent Distributed Environment for Computational Spectroscopy (CODECS)’’ are also acknowledged.

[1] G. N. Lewis, J. Am. Chem. Soc. **46**, 2027 (1924).

[2] M. F. Crawford, H. L. Welsh, and J. L. Locke, Phys. Rev. **75**, 1607 (1949).

- [3] L. Frommhold, *Collision-induced Absorption in Gases* (Cambridge Monographs on Atomic, Molecular and Chemical Physics, Cambridge University Press, 1994), ISBN 9780521393454.
- [4] M. Abel and L. Frommhold, *Can. J. Phys.* **91**, 857 (2013).
- [5] W. Klemperer and V. Vaida, *Proc. Nat. Ac. Sci.* **103**, 10584 (2006).
- [6] M. Bartolomei, E. Carmona-Novillo, M. I. Hernández, J. Campos-Martínez, and R. Hernández-Lamonedá, *J. Chem. Phys.* **128**, 214304 (2008).
- [7] M. Bartolomei, M. I. Hernández, J. Campos-Martínez, E. Carmona-Novillo, and R. Hernández-Lamonedá, *Phys. Chem. Chem. Phys.* **10**, 5374 (2008).
- [8] M. Bartolomei, E. Carmona-Novillo, J. Campos-Martínez, M. I. Hernández, and R. Hernández-Lamonedá, *J. Chem. Phys.* **133**, 12431 (2010).
- [9] M. Bartolomei, E. Carmona-Novillo, M. I. Hernández, J. Campos-Martínez, and R. Hernández-Lamonedá, *J. Comp. Chem.* **32**, 279 (2011).
- [10] L. Gomez, B. Bussery-Honvault, T. Cauchy, M. Bartolomei, D. Cappelletti, and F. Pirani, *Chem. Phys. Lett.* **445**, 99 (2007).
- [11] B. Jeziorski, R. Moszynski, and K. Szalewicz, *Chem. Rev.* **94**, 1887 (1994).
- [12] B. Bussery-Honvault and J.-M. Hartmann, *J. Chem. Phys.* **140**, 054309 (2014), 054309:1-054309:6.
- [13] V. Aquilanti, M. Bartolomei, E. Carmona-Novillo, and F. Pirani, *J. Chem. Phys.* **118**, 2214 (2003).
- [14] P. S. Zuchowski, R. Podaszwa, R. Moszynski, B. Jeziorski, and K. Szalewicz, *J. Chem. Phys.* **129**, 084101 (2008), ISSN 0021-9606.
- [15] A. van der Avoird and G. Brocks, *J. Chem. Phys.* **87**, 5346 (1987).
- [16] R. A. Kendall, T. H. Dunning, and R. J. Harrison, *J. Chem. Phys.* **96**, 6796 (1992).
- [17] F. M. Tao and Y. K. Pan, *J. Chem. Phys.* **97**, 4989 (1992).
- [18] C. Adamo and V. Barone, *J. Chem. Phys.* **110**, 6158 (1999).
- [19] *Dalton, a molecular electronic structure program, release 2.0* (2005), see <http://www.kjemi.uio.no/software/dalton/dalton.html>.
- [20] E. Fermi and G. Amaldi, *Memorie della Classe di Scienze Fisiche, Matematiche e Naturali. R. Accademia D'Italia* **6**, 117 (1934).
- [21] D. J. Tozer and N. C. Handy, *J. Chem. Phys.* **109**, 10180 (1998).
- [22] P. S. Zuchowski, *Chem. Phys. Lett.* **450**, 203 (2008).
- [23] NIST Chemistry WebBook, NIST Standard Reference Database Number 69, ed. P. J. Linstrom and W. G. Mallard, 2007, <http://WebBook.nist.gov>.
- [24] R. Bukowski, W. Cencek, P. Jankowski, M. Jeziorska, B. Jeziorski, S. A. Kucharski, V. F. Lotrich, A. J. Misquitta, R. Moszynski, K. Patkowski, et al., *Sapt2008, version 2008.2, an ab initio program for many-body-symmetry-adapted perturbation theory of intermolecular interaction energies* (2008), see <http://www.physics.udel.edu/~szalewic/SAPT/index.html>.
- [25] S. Boys and F. Bernardi, *Mol. Phys.* **19**, 553 (1970).
- [26] J. H. van Lenthe, J. G. C. M. van Duijneveldt-van de Rijdt, and F. van Duijneveldt, *Adv. Chem. Phys.* **69**, 521 (1987).
- [27] H.-J. Werner, P. J. Knowles, R. Lindh, F. R. Manby, M. Schütz, P. Celani, T. Korona, G. Rauhut, R. D. Amos, A. Bernhardsson, et al., *Molpro, version 2006.1, a package of ab initio programs* (2006), see <http://www.molpro.net>.
- [28] P. E. S. Wormer and A. van der Avoird, *J. Chem. Phys.* **81**, 1929 (1984).
- [29] M. Abramovitz and I. A. Stegun, *Handbook of Mathematical Functions* (Dover, New York, 1972).
- [30] T. Cwiok, B. Jeziorski, W. Kolos, R. Moszynski, J. Rychlewski, and K. Szalewicz, *Chem. Phys. Lett.* **195**, 67 (1992).
- [31] A. van der Avoird, P. E. S. Wormer, F. Mulder, and R. M. Berns, in *Topics in Current Chemistry* (Springer, Berlin, Vol.93, Chapter 1, 1980), pp. 1–51.
- [32] T. G. A. Heijmen, R. Moszynski, P. E. S. Wormer, and A. van der Avoird, *Mol. Phys.* **89**, 81 (1996).
- [33] B. Brunetti, G. Liuti, E. Luzzatti, F. Pirani, and F. Vecchiocattivi, *J. Chem. Phys.* **74**, 6734 (1981).
- [34] D. Cappelletti, F. Pirani, B. Bussery-Honvault, L. Gómez, and M. Bartolomei, *Phys. Chem. Chem. Phys.* **10**, 4281 (2008).
- [35] M. Bartolomei, D. Cappelletti, G. de Petris, M. M. Texidor, F. Pirani, M. Rosi, and F. Vecchiocattivi, *Phys. Chem. Chem. Phys.* **10**, 5993 (2008).
- [36] F. Thibault, D. Cappelletti, F. Pirani, and M. Bartolomei, *J. Phys. Chem. A* **113**, 14867 (2009).
- [37] D. Cappelletti, M. Bartolomei, F. Pirani, and V. Aquilanti, *J. Phys. Chem. A* **106**, 10764 (2002).
- [38] L. I. Schiff, *Phys. Rev.* **103**, 443 (1956).
- [39] F. Pirani and F. Vecchiocattivi, *Mol. Phys.* **45**, 1003 (1982).
- [40] V. Aquilanti, D. Ascenzi, D. Cappelletti, M. de Castro-Vitores, and F. Pirani, *J. Chem. Phys.* **109**, 3898 (1998).
- [41] J. Pérez-Ríos, M. Bartolomei, J. Campos-Martínez, M. I. Hernández, and R. Hernández-Lamonedá, *J. Phys. Chem. A* **113**, 14952 (2009).
- [42] R. B. Bernstein and T. J. P. O'Brien, *Discuss. Faraday Soc.* **40**, 35 (1965).
- [43] R. B. Bernstein and T. J. P. O'Brien, *J. Chem. Phys.* **46**, 1208 (1967).
- [44] J. Pérez-Ríos, M. Bartolomei, J. Campos-Martínez, and M. I. Hernández, *Chem. Phys. Lett.* **522**, 28 (2012), 28–32.
- [45] M. Martin, R. Trengove, K. Harris, and P. Dunlop, *Aust. J. Chem.* **35**, 1525 (1982).
- [46] K. Fostiropoulos, G. Natour, J. Sommer, and B. Schramm, *Ber. Bunsenges. Phys. Chem.* **92**, 925 (1988).
- [47] R. T. Pack, *J. Chem. Phys.* **78**, 7217 (1983).
- [48] P. T. Eubank and K. R. Hall, *AIChE Journal* **36**, 1661 (1990).
- [49] P. R. Bunker, *Molecular Symmetry and Spectroscopy* (Academic Press Inc., 1979).
- [50] S. Green, *J. Chem. Phys.* **62**, 2271 (1975).
- [51] A. van der Avoird, P. Wormer, , and R. Moszynski, *Chem. Rev.* **94**, 1931 (1994).
- [52] J. M. Hutson, *Comp. Phys. Comm.* **84**, 1 (1994).
- [53] M. H. Alexander and A. E. DePristo, *J. Chem. Phys.* **66**, 2166 (1977).
- [54] J. Brown and A. Carrington, *Rotational Spectroscopy of Diatomic Molecules* (Cambridge University Press, 2003).
- [55] BOUND. J. M. Hutson (1993), computer Code, Version 5, distributed by Collaborative Computational Project

- no. 6 of the Science and Engineering Research Council (UK).
- [56] D. E. Manolopoulos, *J. Chem. Phys.* **85**, 6425 (1986).
- [57] B. R. Johnson, *J. Comp. Phys.* **13**, 445 (1973).
- [58] A. E. Thornley and J. M. Hutson, *J. Chem. Phys.* **101**, 5578 (1994).
- [59] V. Aquilanti, D. Ascenzi, M. Bartolomei, D. Cappelletti, S. Cavalli, M. de Castro Vitores, and F. Pirani, *J. Am. Chem. Soc.* **121**, 10794 (1999).
- [60] E. Carmona-Novillo, M. Bartolomei, M. I. Hernández, J. Campos-Martínez, and R. Hernández-Lamoneda, *J. Chem. Phys.* **137**, 114304 (2012).
- [61] V. Aquilanti, M. Bartolomei, D. Cappelletti, E. Carmona-Novillo, and F. Pirani, *J. Chem. Phys.* **117**, 615 (2002).

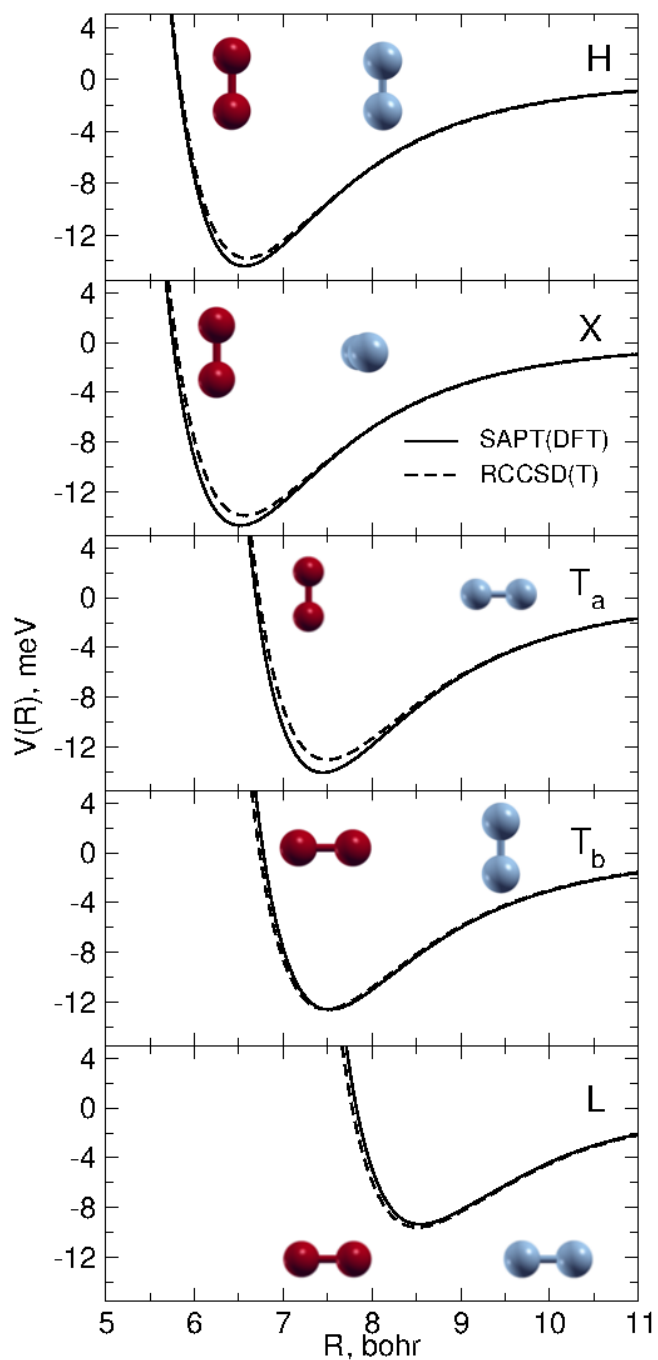


FIG. 1. Comparison between SAPT(DFT) and RCCSD(T) intermolecular potentials at five limiting orientations of O₂-N₂ as obtained by using the aug-cc-pVTZ plus bond function basis set (see text). The different arrangements are depicted in the insets, where O and N atoms are symbolized by red and light blue balls, respectively.

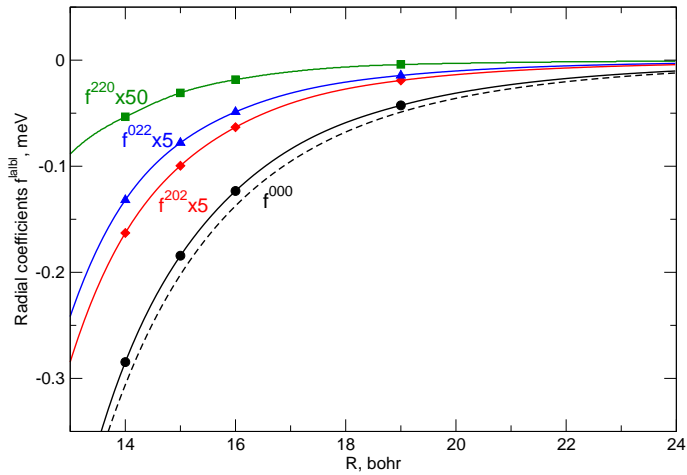


FIG. 2. Behavior of the f^{000} , f^{202} , f^{022} and f^{220} radial coefficients at large intermolecular distances. Points at 14, 15 and 16 bohr are those resulting from the *ab initio* calculations, whereas Eq. (4) is used for $R=19$ bohr. For $R < 19$ bohr the curves are the result of cubic spline interpolation, while for larger R 's they are given by the analytical long range behavior of Eq. 4. The dashed line corresponds to the f^{000} term of the experimentally derived PES of Ref.[13].

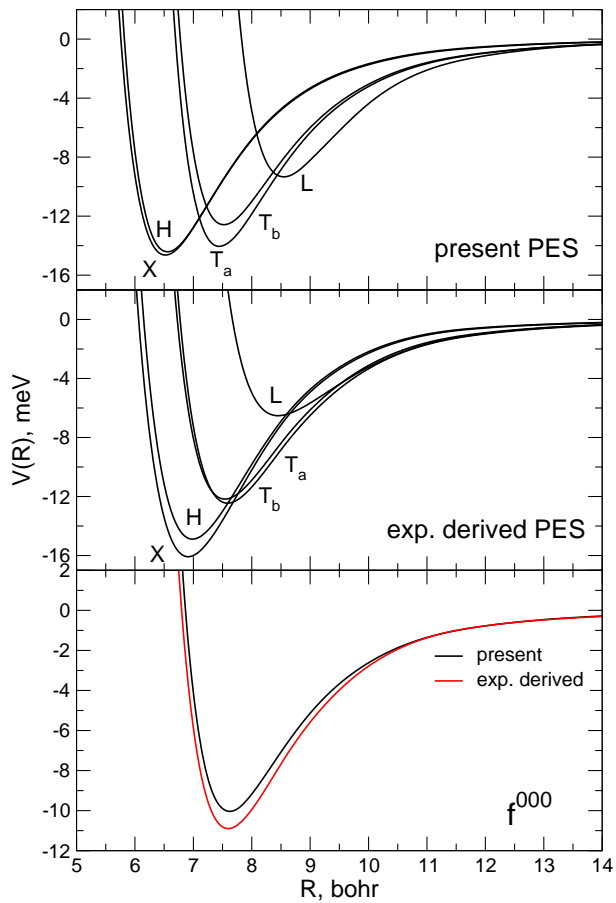


FIG. 3. Comparison between present *ab initio* PES and the experimentally derived one from Ref. [13]. Upper and intermediate panels: potential energy (in meV) profiles as functions of the intermolecular distance R (in bohr) for selected geometries of the dimer. Lower panel: spherical average f^{000} as a function of R .

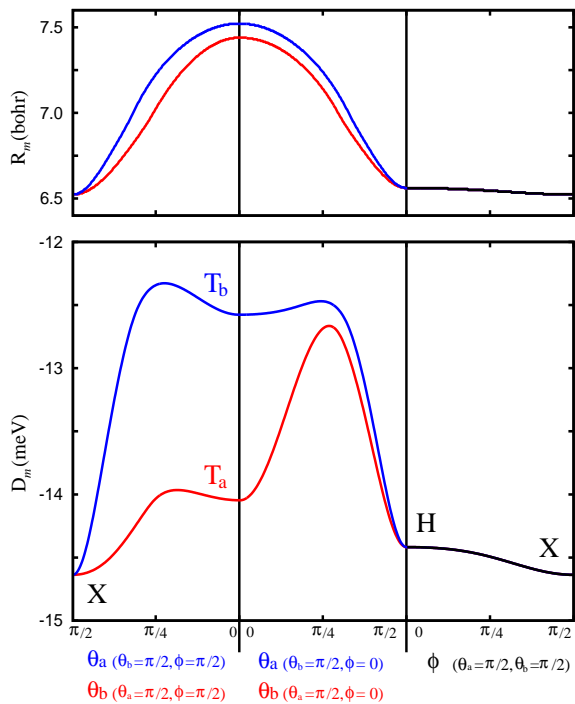


FIG. 4. Low energy pathways of the present $\text{O}_2\text{-N}_2$ PES. As the relative orientation of the diatoms is varied as indicated in the abscissae labels, the associated equilibrium distances R_m (upper panel) and well depths D_m (lower panel) are displayed. Left panels: from the crossed X to T_a and T_b geometries; center panels: from the latter to the H configuration; right panels: from H to the X orientation.

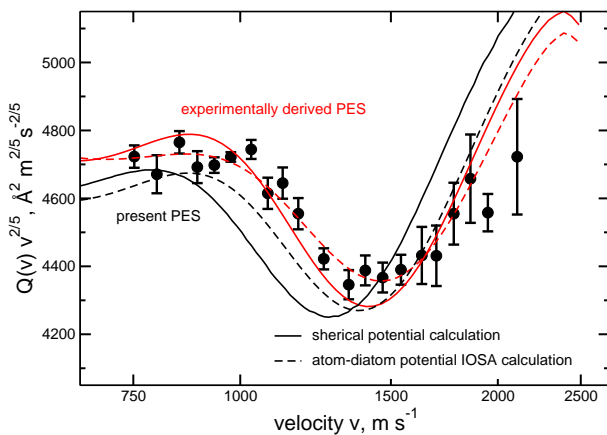


FIG. 5. Total integral cross sections $Q(v)$ times $v^{2/5}$, for scattering of a rotationally hot O_2 effusive beam by N_2 target molecules as functions of the beam velocity, v . Present calculations are in solid and dashed black lines as obtained with a spherical average and an atom-diatom dynamical models, respectively (see text). Experimental data (filled circles with error bars) and related best fit calculations (in red) are from Refs. [13, 33].

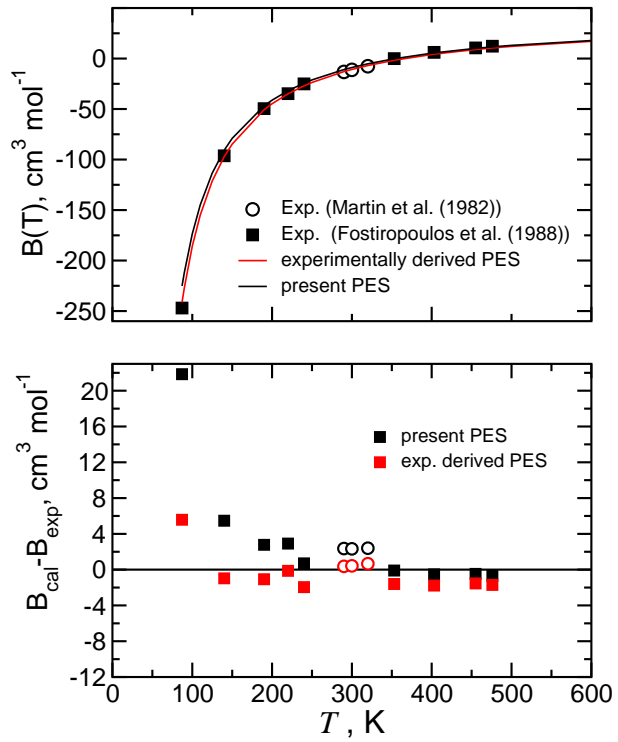


FIG. 6. Upper panel: Second virial coefficients $B(T)$ as a function of temperature. Present calculations are compared with those obtained with the Perugia-PES[13] as well as with the experimental data of Martin *et al* [45] and Fostiropoulos *et al* [46]. Lower panel: Deviations between experimental and calculated $B(T)$'s.

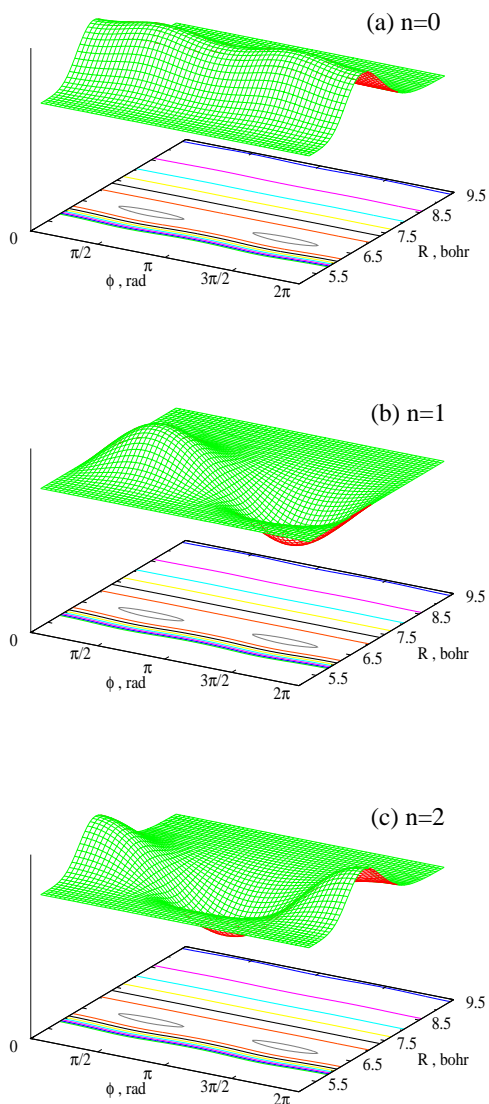


FIG. 7. Wave functions multiplied by R (in arbitrary units) for the lowest vibrational states of $\text{O}_2\text{-N}_2$, as functions of the intermolecular distance R (bohr) and the torsional angle (radian). Contour plots of the PES are also shown in the bottom planes of the plots, with contour lines ranging from -14.5 to -0.5 meV, in steps of 2 meV. In all cases, the bending angles θ_a and θ_b have both been fixed at $\pi/2$. (a) $n = 0$, real part, (b) $n = 1$, imaginary part (c) $n = 2$, real part; (the associated imaginary/real parts are zero).

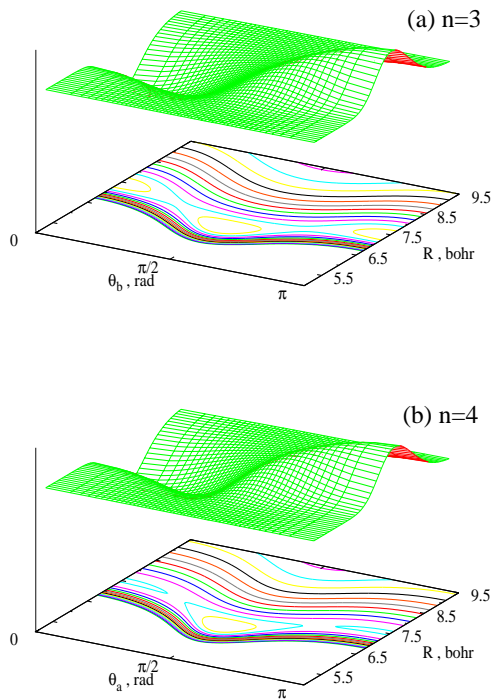


FIG. 8. (a) Real part of the wave function multiplied by R (in arbitrary units) of the third excited rotationless state ($n=3$) of $\text{O}_2\text{-N}_2$, as a function of R (bohr) and θ_b (radian), with the bending angle θ_a fixed at $\pi/2$ and $\phi = 0$. Imaginary part is zero. (b) As in (a), for $n=4$. In this case the wave function is shown versus R and θ_a , with $\theta_b = \pi/2$ and $\phi = 0$. In this way, these states correspond to T_a and T_b configurations, respectively. Contour plots of the PES are also shown in the bottom planes of the plots, with contour lines ranging from -13.5 to -0.5 meV, in steps of 1 meV.